

APPLICATION OF A CONGENER-SPECIFIC DEBROMINATION MODEL TO STUDY  
PHOTODEBROMINATION, ANAEROBIC MICROBIAL DEBROMINATION, AND  $\text{Fe}^0$   
REDUCTION OF POLYBROMINATED DIPHENYL ETHERSXIA ZENG,<sup>†</sup> STACI L. MASSEY SIMONICH,<sup>\*†‡</sup> KRISTIN R. ROBROCK,<sup>§</sup> PETER KORYTÁR,<sup>||</sup> LISA ALVAREZ-COHEN,<sup>§</sup>  
and DOUGLAS F. BAROFSKY<sup>†</sup><sup>†</sup>Department of Chemistry, <sup>‡</sup>Department of Environmental and Molecular Toxicology, Oregon State University, Corvallis, Oregon 97331, USA<sup>§</sup>Department of Civil and Environmental Engineering, University of California, Berkeley, California 94720, USA<sup>||</sup>Wageningen Institute for Marine Resources and Ecosystem Studies, Haringkade 1, 1976 CP IJmuiden, The Netherlands

(Submitted 30 March 2009; Returned for Revision 4 September 2009; Accepted 26 October 2009)

**Abstract**—A model was used to predict the photodebromination of the BDE-203, 197, 196, and 153, the major components of the octa-polybrominated diphenyl ether (PBDE) technical mixture, as well as BDE-47, and the predicted results were compared to the experimental results. The predicted reaction time profiles of the photodebromination products correlate well with the experimental results. In addition, the slope of the linear regression between the measured product concentrations of the first step of the photodebromination products and their enthalpies of formation was found to be close to their theoretical value. The photodebromination results of the octa-BDE technical mixture were compared with anaerobic microbial debromination results and were found to be the same in both experiments. The debromination pathways of technical octa-BDE mixture were identified and BDE-154, 99, 47, and 31 were found to be the most abundant hexa-, penta-, tetra-, and tri-BDE debromination products, respectively. In addition to photodebromination and anaerobic biodebromination, the model prediction was also compared to the zero-valent iron reduction of BDE-209, 100, and 47 and the same debromination products were observed. Good correlation was observed between the photodebromination rate constants of fifteen PBDE congeners and their calculated lowest unoccupied molecular orbital (LUMO) energies, indicating that PBDE photodebromination is caused by electron transfer. Furthermore, the rate constants for the three different PBDE debromination processes are controlled by C–Br bond dissociation energy. With the model from the present study, the major debromination products for any PBDE congener released into the environment can be predicted. Environ. Toxicol. Chem. 2010;29:770–778. © 2010 SETAC

**Keywords**—Polybrominated diphenyl ether Model Photodegradation Anaerobic microbial debromination

## INTRODUCTION

The environmental fate of polybrominated diphenyl ethers (PBDEs) continues to be extensively studied even after penta-BDE and octa-BDE were banned in Europe and voluntarily phased out in the United States because of their toxicity and persistence [1,2]. In addition, these higher brominated BDE mixtures have been shown to degrade by sunlight and microorganisms to lower brominated BDE congeners [3–10].

Several biotic and abiotic transformation reactions of PBDEs have been studied. Photodebromination is one of the major abiotic transformation mechanisms in the environment, and PBDEs have been shown to photodebrominate by both artificial and natural sunlight [3–6]. Anaerobic biodebromination also results in lower brominated PBDE products [7]. The octa-BDE technical mixture, which was widely used and classified as a teratogen [11], was reported to undergo stepwise debromination in *Dehalococcoides*-containing cultures to produce the more toxic BDE-154, BDE-99, BDE-49, and BDE-47 congeners [8]. Brominated diphenyl ether-209, the fully brominated PBDE, was also reported to biodegrade anaero-

bically to lower brominated diphenyl ethers in sewage sludge [9,10] and by a pure culture [8].

Zero-valent iron metal ( $\text{Fe}^0$ ) has been studied for the remediation of polyhalogenated organic compounds such as tetrachloromethane, 1,1,1-trichloroethane, tetrachloroethene, and PBDEs, and first-order reaction rates were found to govern these reactions [12,13]. A linear correlation between the rate constants for  $\text{Fe}^0$  dehalogenation and the PBDE congener lowest unoccupied molecular orbital (LUMO) energies has been reported [13].

The three different PBDEs debromination processes, photodebromination, anaerobic biodebromination, and  $\text{Fe}^0$  reduction, all involve first-order, stepwise debromination reactions, and similar debromination products for these three debromination processes have been reported [3,10,13]. A previous study reported that the photodebromination and anaerobic biodebromination of BDE-15 (4,4'-BDE) followed the same debromination pathway and produced BDE-3 (4-BDE) and diphenyl ether in a stepwise manner [7]. Neither rearrangement of Br or C–O bond cleavage was found in the above reactions. This suggests that photochemical and biotic debromination of PBDEs obeys similar degradation kinetics.

To test the hypothesis that photochemical, biological, and chemical debromination of PBDEs are governed by the same reaction mechanism, congener-specific studies were conducted in the present work to compare the different PBDE

\* To whom correspondence may be addressed (staci.simonich@oregonstate.edu).

Published online 8 January 2010 in Wiley InterScience (www.interscience.wiley.com).

debromination processes. Using a theoretical model we developed previously, we predicted the photodebromination of PBDEs based on the difference in bromine dissociation energies between PBDE congeners [14]. Theoretically, if the reaction debromination mechanisms are the same, the model should also predict anaerobic biodebromination and Fe<sup>0</sup> reduction of PBDEs.

Four of the major components of the octa-BDE technical mixture, BDE-203 (7.6%), 197 (29.6%), 196 (3.8%), and 153 (2.2%), were studied because of their large volume use and relatively high degree of bromination. The photodebromination experiments of BDE-183 (41.3%) and BDE-207 (15.1%) were not performed due to the lack of pure standards at the time of the experiments. In addition to these congeners, BDE-99 and 47, two of the most frequently detected congeners in the environment, were included in the present study. The photodebromination of the octa-BDE technical mixture was studied and compared with the results of the anaerobic biodebromination experiments and model predictions. The model predicted products, their concentrations, and the reactant debromination rate constants were also compared to the experimental results. Using the photodebromination model, the relationship between the relative debromination rates and the LUMO energies of the PBDEs was investigated.

## EXPERIMENTAL SECTION

### Chemicals

A standard mixture of 39 PBDEs was obtained from Cambridge Isotope [15]. Individual standards of BDE-47, 99, 100, 121, 140, 146, 148, 153, 168, 184, 196, 197, 203, 206, 207, and 208 were purchased from AccuStandard. Brominated diphenyl ether-209 and the octa-BDE technical mixture were purchased from Sigma Aldrich. The PBDE standard containing 126 congeners that was used to identify the PBDE debromination products was provided by Peter Korytár [16].

### Photodebromination experiments

The photodebromination experiments described here were conducted on new congeners (BDE-203, 197, 196, 153, and 47) and technical mixtures (octa-BDE). The experimental conditions used have been previously described [14]. Briefly, the photodebromination experiments were conducted using a Rayonet RPR-100 photochemical reactor with RMR-2537A (254 nm,  $2.7 \times 10^{-8}$  mol/s/cm<sup>3</sup>) ultraviolet (UV) lamps purchased from Southern New England Ultraviolet Company. The photochemical reactor was measured 16 inches (40.6 cm) high and 12 inches (30.5 cm) square, the reactor barrel was 10 inches (25.4 cm) in diameter by 15 inches (38.1 cm) deep, and the temperature was approximately 35°C inside the reactor with the fan in operation. The PBDE congeners and octa-BDE technical mixture were dissolved in 10 ml isoctane, and these solutions were irradiated in sealed quartz vials. The irradiated samples were collected at different time intervals and analyzed using a JEOL (Japan Electron Optics Laboratory) GC mate II gas chromatograph-high resolution mass spectrometer (GC-HRMS) in electron capture negative ionization (ECNI) mode. The GC column was a 30 m J&W (J&W Scientific) DB-5 column (0.25 mm inside diameter and 0.25 μm film thickness), and the GC temperature program was:

100°C (hold for 1 min); 10°C/min to 320°C (hold for 27 min). The temperatures of the splitless injector, GC interface, and ion source were 280, 250, and 250°C, respectively. The PBDE congener concentrations were quantified using external calibration. Polybrominated diphenyl ether congeners without available standards were quantified using the average ECNI response of the homologous PBDE group. Previously developed GC retention time model [14] and the pure PBDE standards were used to identify the photodebromination products.

### Anaerobic biodebromination experiments

The anaerobic biodebromination experimental conditions have been previously described [17], and these experiments were conducted on BDE-196, 203, 197, 183, 153, 99, and 47 at the University of California-Berkeley (California, USA). The anaerobic biodebromination of these PBDE congeners was performed on a trichloroethylene-dechlorinating enrichment culture containing multiple *Dehalococcoides* strains designated ANAS *Dehalococcoides*-organism-containing microbial consortium (referred to as ANAS) that was mixed in a 1:10 ratio with *Dehalococcoides ethenogenes* 195 (ANAS195), a tetrachloroethene to dichloroethene dechlorinating bacterium *Dehalobacter restrictus* PER-K23 culture, and a pentachlorophenol (PCP) degrading bacterium *Desulfitobacterium hafniense* PCP-1 culture. All cultures were grown in 160-ml serum bottles filled with 100-ml anaerobic minimal medium and sealed with blue butyl rubber septa with 20 μg/L individual PBDE congeners and the respective chlorinated substrate [17]. The medium was made anaerobic by flushing with a continuous stream of nitrogen gas and reduced with 0.2 mM cysteine sulfide. An oxygen indicator, resazurin, was also added to ensure that the cultures remained anaerobic. All samples and controls were incubated at 30°C in the dark without shaking and experiments were conducted with triplicate biological samples and were repeated to confirm the results. Polybrominated diphenyl ether congeners were detected using two-dimensional chromatography at the Wageningen IMARES Laboratories in IJmuiden, The Netherlands. An Agilent 6890 gas chromatograph equipped with an electron capture detector and a loop-type carbon dioxide jet was employed for analysis. Previously collected data were reanalyzed to obtain kinetics profiles of byproduct formation to compare with photolytic debromination and Fe<sup>0</sup> reduction.

### PBDE debromination model

The PBDE debromination model has been described previously [14]. The same model was used to compare PBDE photodebromination, biodebromination, and Fe<sup>0</sup> debromination, using reaction rates relative to BDE-209 [14]. For the debromination of the octa-BDE technical mixture, individual debromination models were developed for each PBDE congener in the technical mixture and the individual congener models were summed.

## RESULTS AND DISCUSSION

### Photo and microbial debromination of selected PBDEs

The reaction time profiles of both the experimental and model predicted photodebromination results for BDE-47,

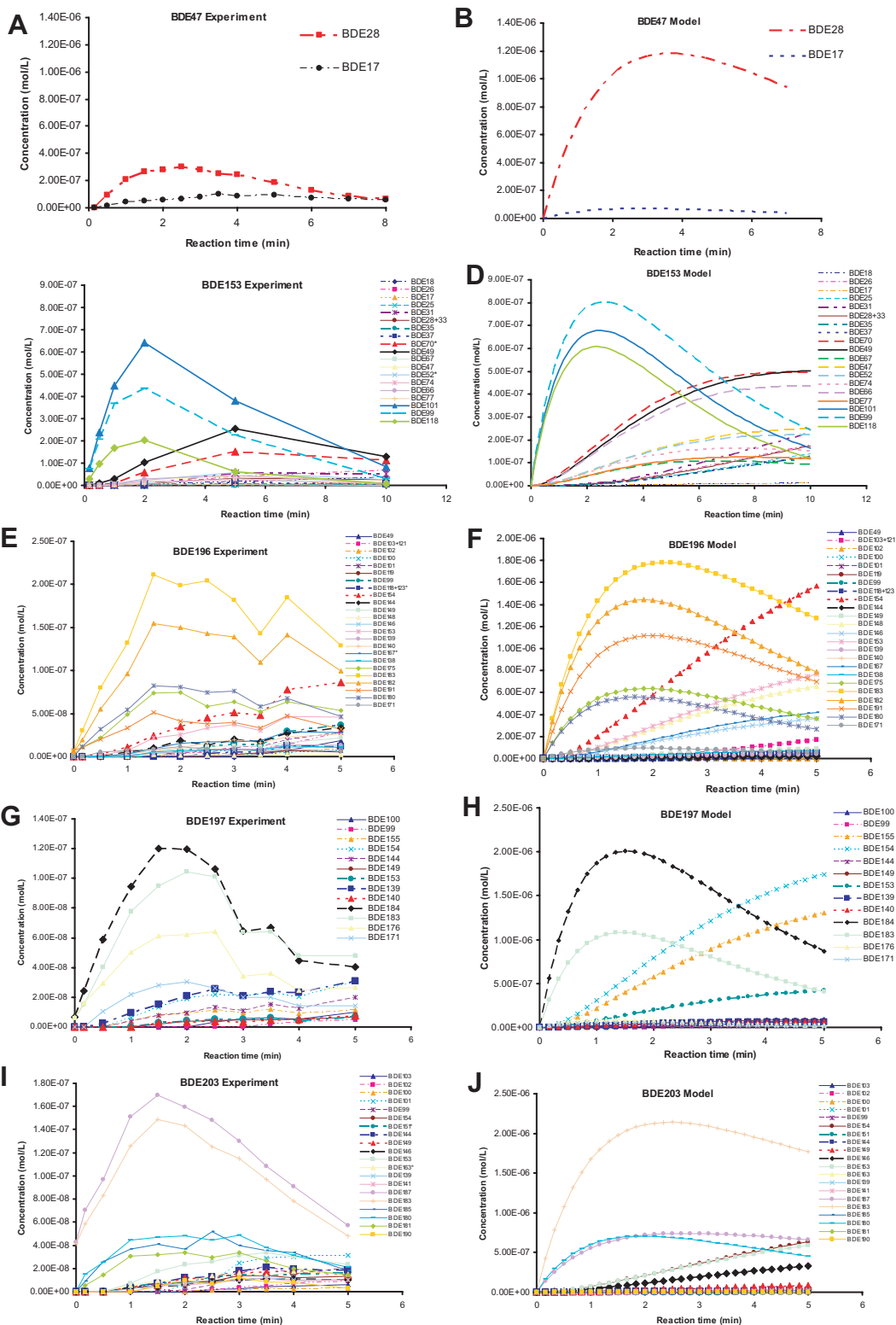


Fig. 1. Predicted and experimental reaction time profiles for brominated diphenyl ether (BDE)-47, 153, 196, 197, and 203 photodebromination products. Note the difference in scale on the y axis. [Color figure can be seen in the online version of this article, available at [www.interscience.wiley.com](http://www.interscience.wiley.com).]

153, 196, 197, and 203 are shown in Figure 1. The correlations between the experimental results and the model predictions are shown in the Supplemental Data, Figure S1. Diphenyl ether was not monitored in all the experiments.

The BDE-47 photodebromination experiments produced two tri-BDEs, BDE-28, and BDE-17 (Fig. 1A). These exper-

imental results were confirmed by the model prediction (Fig. 1B and Supplemental Data, Fig. S1A). Both the model and the experimental result showed that during the reaction BDE-28 (2,4',4'-triBDE), an *ortho* debromination product of BDE-47, showed a higher concentration than BDE-17 (2,2',4'-triBDE), a *para* debromination product of BDE-47. This indicates that the

*ortho* bromine on BDE-47 is less stable and more labile under UV light than the *para* bromine of BDE-47. This is consistent with our previous study where it was determined that, on the same aromatic ring of a diphenyl ether, the *ortho* bromine was 6.86 kJ/mol lower in energy than the *para* bromine [18]. The reaction time profile for the experimental photodebromination of BDE-47 indicated that BDE-28 reached its maximum concentration at 2.5 min (Fig. 1A), whereas the model predicted a maximum concentration at 3.7 min (Fig. 1B). This difference is also shown in the Supplemental Data, Figure S1A. The correlation between the predicted and experimental concentrations of BDE-28 and BDE-17 were statistically significant ( $p < 0.05$ ). The slope of the linear regression between the predicted and experimental results for BDE-47 photodebromination to BDE-28 was much higher (4.19) than for BDE-17 (0.86) (Supplemental Data, Fig. S1A). This indicates the BDE-28 concentration was overestimated by the model, most possibly due to the estimation error in model simulation [14]. No di- or mono-BDEs were detected in this experiment, and this may be due to their reduced sensitivity by GC/ECNI-MS [14]. In the anaerobic microbial experiments, BDE-17 was the major product of the first debromination step. In the ANAS195 culture, BDE-28 was produced in minor concentrations, whereas in the *D. restrictus* and *D. hafniense* cultures BDE-17 immediately debrominated further to BDE-4. Steric hindrance is a probable explanation for the difference between the photo and biodebromination because production of BDE-28 involves an *ortho* bromine removal compared to the *meta* bromine removal step required to produce BDE-17.

Brominated diphenyl ether-153, the only hexa-BDE in the octa-BDE technical mixture, photodegraded to three penta-BDE congeners, including BDE-101, 99, and 118 (Fig. 1C). The most abundant tetra-BDE photodebromination product was BDE-49, followed by two other tetra-BDE congeners, which were identified as BDE-70 and BDE-52 (Fig. 1C). The photodebromination experimental results for BDE-153 follow a similar profile as the photodebromination model predictions and the penta-BDE photodebromination products reached their maximum concentration at approximately 2 min in both cases (Fig. 1C and D). The slopes of the least-squares regression of the predicted product concentrations and the experimental concentrations were similar for the BDE-153 photodebromination products (Supplemental Data, Fig. S1C). In addition, the correlations were statistically significant ( $p < 0.05$ ) for all of the BDE-153 photodebromination products except for BDE-49 ( $p = 0.058$ ). This discrepancy was the result of the model predicting that the concentration of BDE-49 would peak at 10 min (Fig. 1D), whereas the experiment results showed a peak in concentration at 5 min (Fig. 1C). Microbial debromination of BDE-153 also resulted in the formation of BDE-99 and 101 as major penta brominated products. However, BDE-118 was only minor biodebromination product for one bacterial species—ANAS195 (Fig. 2). The proportions of BDE-99 and 101 differed between the cultures, with BDE-99 dominating in two species and BDE-101 in the other. Again, steric hindrance is probably the cause of why the *ortho* debromination product *penta* BDE-118 was not produced in more abundance.

Brominated diphenyl ether-182 and 183 were the most abundant hepta-BDE photodebromination products of BDE-196, in both the experimental results (Fig. 1E) and the model

prediction (Fig. 1F). The model prediction and the experimental results also showed that BDE-154 and 153 were the most abundant hexa-BDE photodebromination products of BDE-196 (Fig. 1E and F). The model predicted relative concentrations for the BDE-196 photodebromination products matched the experimental data well and the correlations between them were all statistically significant for all the major photodebromination products (Supplemental Data, Fig. S1D). However, the concentrations from experiment were one order of magnitude lower than the model prediction. Brominated diphenyl ether-182 and 183 were also important anaerobic biodebromination products of BDE-196, although the hepta BDE-175 was also produced at equivalent or higher concentrations to BDE-182 and BDE-183 (Fig. 2). It is unclear why BDE-175 would be such an abundant anaerobic biodebromination product given that it is less stable than BDE-182 and BDE-183. It is possible that this reaction is catalyzed by microbial enzymes. Each of the microbial cultures were able to produce one of the two *ortho*-substituted debromination products, either BDE-180 or BDE-191, and, similar to photodebromination, these products were present at lower concentrations (Fig. 2).

The experimentally determined photodebromination product time profile for BDE-197 (Fig. 1G) was also well predicted by the photodebromination model (Fig. 1H). Brominated diphenyl ether-184 and 183 were predicted to be the most abundant hepta-BDE products, and this was confirmed by the experimental results. However, BDE-176 was predicted by the model to be much lower in concentration than BDE-184 (Fig. 1H) but was measured at a comparable concentration to BDE-184 in the experiment (Fig. 1G). This is also shown in the correlation between the predicted and experimentally determined product concentrations (Supplemental Data, Fig. S1E), where the slope of the linear regression is much lower for BDE-176 than it is for other BDE-197 photodebromination products. Two of the microbial species *D. restrictus* and ANAS195 produced the hepta-BDE congeners, 184, 183, and 176, in the same proportions (Fig. 2). However, the third species, *D. hafniense*, produced more BDE-183 than BDE-176 (Fig. 2). It is interesting to note that the microorganisms did not have difficulty catalyzing the removal of one of the *ortho* bromines of BDE-197 to produce BDE-183. However, BDE-171 was not a product. This suggests that the other unflanked *ortho* bromine of BDE-197 could not be removed by the microorganisms. From polychlorinated biphenyl and dioxin microbial dechlorination literature, it has been shown that microorganisms prefer to remove flanked than unflanked halogens [19,20]. A comparison between the model prediction, photodebromination, and anaerobic biodebromination of BDE-197 is shown in the Supplemental Data, Figure S2. All the data of concentration were shown in percent (%) relative to total PBDE concentration.

Brominated diphenyl ether-187, 185, and 180, all hepta-BDE congeners, were identified as BDE-203 photodebromination products in the experiments (Fig. 1I). Quantification of these congeners was accomplished by using the average ECNI response for the hepta-BDEs. Brominated diphenyl ether-180, 187, and 183 were predicted by the model to be the most abundant BDE-203 photodebromination products and BDE-183 was predicted to have the highest concentration (Fig. 1J). However, the experimental results showed that BDE-187 had

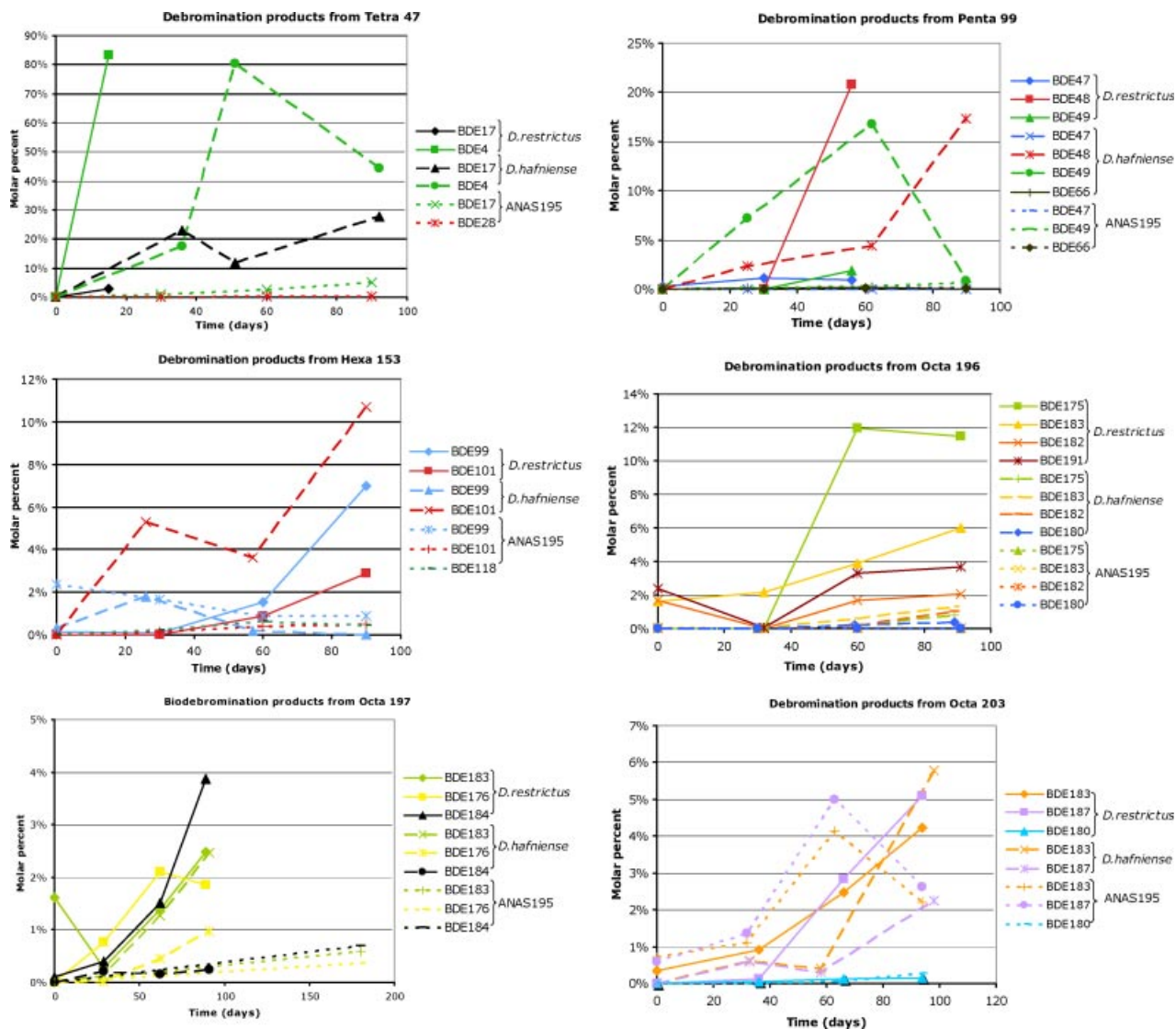


Fig. 2. Reaction time profiles for brominated diphenyl ether (BDE)-47, 99, 153, 196, 197, and 203 anaerobic biodebromination products. [Color figure can be seen in the online version of this article, available at [www.interscience.wiley.com](http://www.interscience.wiley.com).]

the highest concentration, followed by BDE-183 (Fig. 11). This is also shown in Supplemental Data, Figure S1F, where the slope of BDE-187 correlation (4.76) is lower than that of BDE-183 (15.9). In addition, the predicted maximum concentration time for both BDE-187 and BDE-183 were later than determined by the experiment (Supplemental Data, Fig. S1F). Of the six possible debromination products of BDE-203, the anaerobic biodebromination resulted in the same hepta-BDE congeners as the photodebromination (BDE-183, BDE-187, and BDE-180) (Fig. 2). In two of the microbial cultures *D. restrictus* and ANAS195, BDE-187, and BDE-183 were produced in equal concentrations (Fig. 2). In the third microbial culture, *D. hafniense*, BDE-183 was the dominant product. Hepta BDE-180 was not a product of all of the microbial cultures and, if produced, was present at low concentration (Fig. 2).

Finally, photodebromination of BDE-99 was summarized in an earlier work [14]. The experimental and model predicted primary photodebromination products, BDE-47, BDE-49, and BDE-66 were well correlated [14]. These congeners were also found in the anaerobic biodebromination experiments in all

three microbial cultures (Fig. 2) except that BDE-66 was not found in *D. restrictus*. However, BDE-48, a tetra congener not found in the photodebromination experiments and predicted at very low level by the model (<0.6% at any time), was produced by microorganisms in two of the cultures (*D. restrictus* and *D. hafniense*).

#### Octa-BDE technical mixture debromination and reaction pathways

The PBDE congeners discussed above, except BDE-47 and 99, are all major components of the octa-BDE technical mixture. The photodebromination reaction pathways of BDE-203, 197, 196, 153, and 47 are summarized in Figure 3A–E. By adding the congener specific photodebromination reactions together, the photodebromination of the octa-BDE technical mixture can be estimated and compared to its experimental photodebromination.

The photodebromination reaction time profiles by congener for the octa-BDE technical mixture reactants and products are shown in the Supplemental Data, Figure S3A and C, respec-

tively, for the experimental results and in the Supplemental Data, Figures S-3B and D for the model prediction. No mono- or di-BDEs were detected in the photodebromination experiment. The model prediction was based on the first-order experimental photodebromination rate constant for BDE-207 ( $1.536 \text{ min}^{-1}$ ), because it is the only congener that is not the debromination product of other congeners. Because all the other congeners studied in the octa-BDE photodebromination, except BDE-207, were both parent compounds and products of debromination, the first-order kinetics do not apply to their observed debromination rates. In both the experimental results and model predictions, BDE-154, BDE-99, and BDE-49 were the most abundant hepta-, hexa-, and tetra-BDE products of the octa-BDE technical mixture photodebromination, respectively. Compared to the experimental results, concentration of BDE-154 overestimated in the model.

The reaction time profiles for PBDE congeners by homologous group were shown in the Supplemental Data, Figure S3C for experiment and in the Supplemental Data, Figure S3D for model prediction. The cumulative experimental concentrations for BDE-154, 99, 49, and 47 are shown in the Supplemental Data, Figure S4A and compared with the model prediction in the Supplemental Data, Figure S4C. The cumulative experimental concentrations by homologous group are also plotted in the Supplemental Data, Figure S4B and compared with model predictions in the Supplemental Data, Figure S-4D. At the first 10 min of the experiment, the model predicted the order of concentration (hexa > hepta > penta > tetra), which was close to the experiment. The experimental PBDE concentrations decreased after 10 min in the reaction compared to the model predicted concentrations. The decrease of total mass may be due to the generation of the mono- and di-BDEs, which have very low sensitivities on ECNI. Also, the accumulation of PBDEs on the walls of the reaction tube, the cleavage of ether bond, and/or the formation of PBDFs (polybrominated dibenzo-*p*-furans), although not detected, may also account for the mass loss. The photodebromination for octa-BDE technical mixture is far more complicated than a single PBDE congener. The model could be improved if factors, such as ECNI sensitivity and loss of total mass, could be estimated and incorporated into the model.

In a previous study, the anaerobic biodebromination of the octa-BDE technical mixture produced several lower brominated diphenyl ethers, and BDE-184, 154, 153, 155, 99, 47, and 49 were among the most abundant positively identified products after 322 d of biodebromination [8,17]. The anaerobic biodebromination reactions were much slower than the photodebromination reactions. The relative photodebromination product abundances after 5 min reaction (Supplemental Data, Fig. S4) were very similar to the anaerobic biodebromination product abundances after 322 d (Supplemental Data, Fig S5), where the relative concentrations were BDE-154 > BDE-99 > BDE-49 > BDE-47 and hexa-BDE > hepta-BDE > penta-BDE > tetra-BDE for both debromination processes. The similarity in photodebromination and anaerobic biodebromination products of the octa-BDE technical mixture suggest that these debromination processes share similar reaction mechanisms.

The photodebromination reaction pathways of the octa-BDE technical mixture are summarized in Figure 3F. Brominated diphenyl ether-154, a debromination product of BDE-207,

BDE-203, BDE-196, and BDE-183, is the most abundant hexa-BDE product of the photodebromination of the octa-BDE technical mixture. Brominated diphenyl ether-99, a debromination product of BDE-154 and BDE-153, is the most abundant penta-BDE product, while BDE-49 and BDE-31 are the most abundant tetra and tri-BDE debromination products, respectively. These predominant PBDE photodebromination products were also measured as anaerobic biodebromination products, except for BDE-31 [8], probably due to the slow rate of anaerobic biodebromination. These congeners are likely to be the most abundant products in their homologous groups when the octa-BDE technical mixture degrades in the environment. BDE-99 and 154 are also major components of penta-BDE technical mixture.

#### Comparison to zero-valent iron reduction of PBDEs

The  $\text{Fe}^0$  debromination of BDE-47 was previously studied [13]. The debromination of BDE-47 by zero-valent iron was similar to photodebromination, with similar kinetic profiles for BDE-17 and BDE-28 production. However, there were substantial differences between the zero-valent iron and biological debromination. Both photo and iron-catalyzed debromination of BDE-47 produced BDE-28 at a higher concentration than BDE-17. However the anaerobic biodebromination of BDE-47 resulted in very low concentrations of BDE-28. Brominated diphenyl ether-17 was the major anaerobic biodebromination product of BDE-47 and it was quickly degraded to BDE-4 (Fig. 2). Supplemental Data, Figure S6 shows a comparison between the model predicted debromination, photodebromination, anaerobic biodebromination, and iron catalyzed debromination of BDE-47. All the data of concentration were shown in percent (%) relative to total PBDE concentration.

The debromination of BDE-209, 100, 66, 28, and 7 by  $\text{Fe}^0$  was also previously studied [13]. These results indicated step-wise accumulation to lower brominated BDE congeners, similar to photodebromination and anaerobic biodebromination. All of the BDE-209  $\text{Fe}^0$  debromination products were previously measured in our photodebromination experiments at relatively high concentrations within their homologous groups [14]. The reaction time profiles for the BDE-209  $\text{Fe}^0$  debromination products are shown in Supplemental Data, Figure S7A. For comparison, the corresponding data for the photodebromination of BDE-209 is shown in the Supplemental Data, Figure S7B. The BDE-100  $\text{Fe}^0$  debromination products, 47, 50, 51, and 75, were all measured products in the photodebromination experiments.

#### Relationship between $\Delta H_f$ and concentration of first step debromination products

Because the photodebromination of PBDEs is a first order reaction [3]:

$$-\frac{d[h]}{dt} = k_h[h] \quad (1)$$

then

$$k_h = \sum_i (\alpha_{hi} k_h^i) \quad (2)$$

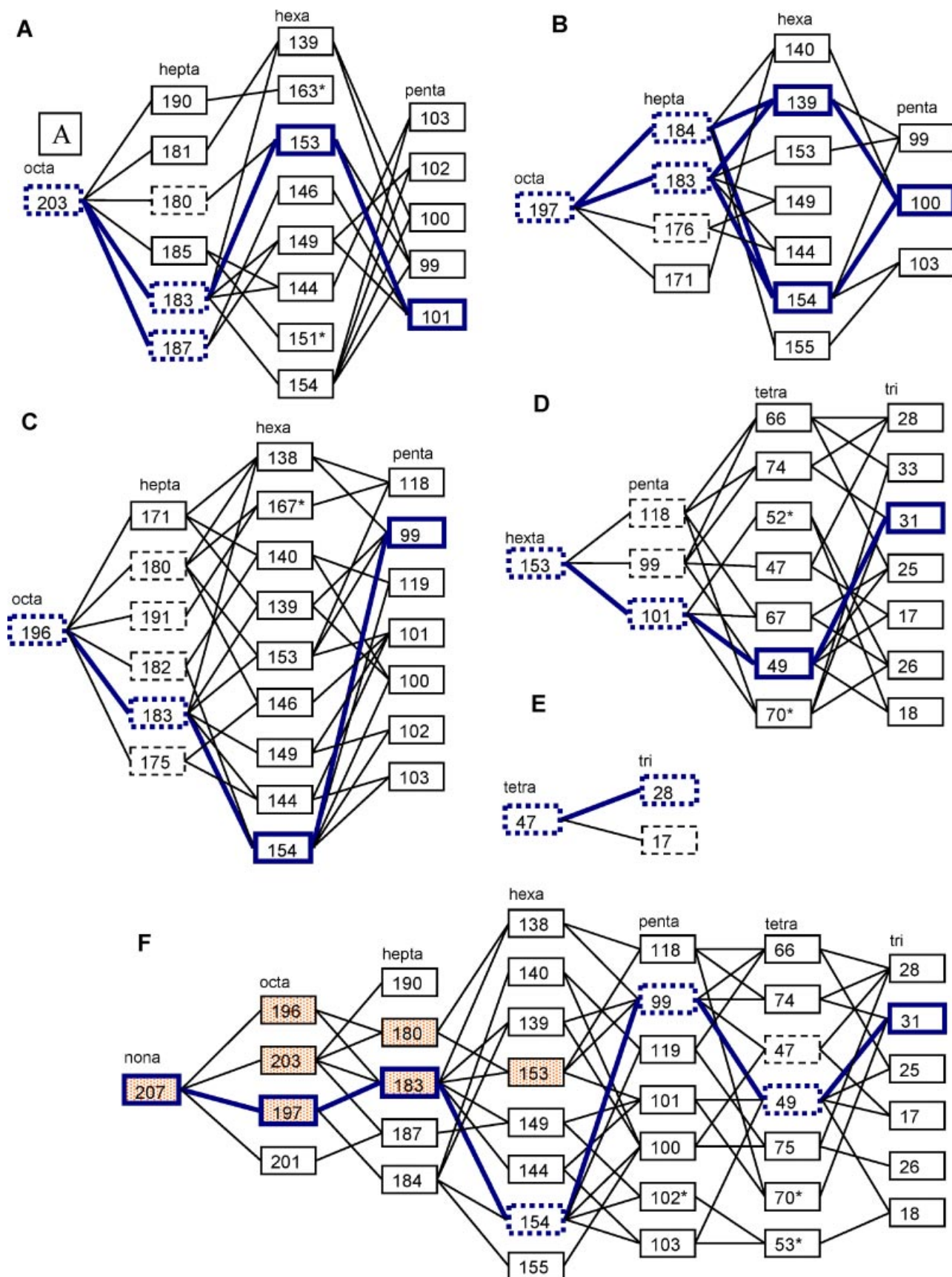


Fig. 3. Photodebromination reaction pathways for brominated diphenyl ether (BDE)-203, 197, 196, 153, 47, and octa-BDE technical mixture. The thick blue colored lines and boxes represent a higher concentration of polybrominated diphenyl ether congeners. The shaded boxes represent the components of the octa-BDE technical mixture. All the boxes represent photodebromination products. The dashed boxes represent products also found in the anaerobic biodebromination studies. [Color figure can be seen in the online version of this article, available at [www.interscience.wiley.com](http://www.interscience.wiley.com).]

where  $[h]$  is the concentration of the parent PBDE congener  $h$ ,  $k_h$  is the debromination rate constant of PBDE congener  $h$ ,  $k_h^i$  is the rate constant for the debromination of  $h$  to  $i$ , and  $\alpha_{hi}$  is the number of reaction pathways for the debromination of  $h$  to  $i$  [14]. The reduced amount of the reactant ( $h$ ) is equal to the increased amount of the debromination products in the first step of the reaction:

$$-d[h] = \sum_i d[i] \quad (3)$$

For each individual product ( $i$ ), the increased amount can be calculated by:

$$\frac{d[i]}{dt} = \alpha_{hi} k_h^i [h] \quad (4)$$

In the initial stages of the debromination, assuming  $[h]$  is constant, Equation 4 becomes:

$$\Delta[i] = \alpha_{hi} k_h^i [h] \Delta t \quad (5)$$

Because the initial concentration of the PBDE products is 0 mol/L and the starting time is 0 s, Equation 5 becomes:

$$[i] = \alpha_{hi} k_h^i [h] t \quad (6)$$

and the natural logarithm of Equation 6 becomes:

$$\ln \frac{[i]}{\alpha_{hi}} = \ln k_h^i + \ln([h]t) \quad (7)$$

Furthermore, the difference in the enthalpy of formation,  $\Delta H_f$ , between two debromination products in exponential format is correlated to the ratio of their individual rate constant [14]:

$$\frac{k_h^i}{k_h^j} = \exp\left(\frac{\Delta H_{fi} - \Delta H_{fj}}{-RT}\right) \quad (8)$$

where  $i$  and  $j$  represent the two different debromination products, and the natural logarithm of both sides of Equation 8 is:

$$\ln k_h^i - \ln k_h^j = \frac{\Delta H_{fi} - \Delta H_{fj}}{-RT} \quad (9)$$

Therefore, for the debromination products in the first step of the debromination, the slope of linear regression between  $\ln k$  and  $\Delta H_f$  should be  $-\frac{1}{RT}$ . According to Equation 7,  $\ln \frac{[i]}{\alpha_{hi}}$  should also correlate with  $\Delta H_f$ , and the slope of the linear regression should also be  $-\frac{1}{RT}$ , which equals  $-0.4036$  when the gas constant  $R$  is 8.314 J/molK, reaction temperature  $T$  is 298 K, and the units for  $\Delta H_f$  are kJ/mol.

The correlation between  $\ln \frac{[i]}{\alpha_{hi}}$  and  $\Delta H_f$  for the first step photodebromination products of BDE-47, 99, 153, 196, 197, and 203 are shown in the Supplemental Data, Figure S8; where  $[i]$  is the measured concentration in the photodebromination experiment. The slopes in the plots in the Supplemental Data, Figure S8 are negative and range from  $-0.07$  to  $-1.37$ , which, for kinetic data, is reasonably close to the theoretical value of  $-0.4036$ . This suggests that the generation rates of debromination products are controlled by their enthalpies of formation and that the model describes the experimental results well. However, due to the limited number of first step photodebro-

mination products, the correlations between  $\ln \frac{[i]}{\alpha_{hi}}$  and  $\Delta H_f$  were not very good. Furthermore, the values of heat of formation were calculated in gas phase. The uncertainty associated with the use of gas-phase data to the liquid phase could also impair the correlations between  $\ln \frac{[i]}{\alpha_{hi}}$  and  $\Delta H_f$ .

The correlations between  $\ln \frac{[i]}{\alpha_{hi}}$  and  $\Delta H_f$  for the first step anaerobic biodebromination products are shown in the Supplemental Data, Figure S9. The concentration of biodebromination products relative to the total PBDE concentration was measured every 30 d. Brominated diphenyl ether-17, a *para*-substituted debromination product, was the only anaerobic biodebromination product of BDE-47 measured in the *D. hafniense* and *D. restrictus* cultures. However, BDE-17 and small amount of BDE-28, an *ortho* debromination product, were measured in the ANAS195 culture from the biodebromination of BDE-47. These results are significantly different from the BDE-47 photodebromination results (Supplemental Data, Fig. S8A), where BDE-28 was measured at a higher concentration than BDE-17. In photodebromination, the C–Br bond in the *ortho* position of BDE-47 is easier to break than the C–Br bond in the *para* position. However, the opposite is true in anaerobic biodebromination, possibly because of steric effects in the *ortho* position. The slopes for the linear regressions for the BDE-99, 153, 183, 196, 197, and 203 anaerobic biodebromination products shown in the Supplemental Data, Figure S9, in most cases, are negative and range from  $-0.0788$  to  $-6.535$ . These slopes are similar, but slightly higher than, the slopes for the photodebromination products. This indicates that the anaerobic biodebromination rate is controlled by the enthalpy of formation, but also by the type of microbial culture and steric effects.

The linear regressions between the natural logarithm of the  $\text{Fe}^0$  debromination product relative concentration per reaction pathway and the  $\Delta H_f$  of the corresponding debromination products are shown in the Supplemental Data, Figure S10. The slopes for the BDE-100, 47, and 28 debromination products are negative and higher than the theoretical value of  $-0.4036$ , ranging from  $-0.0339$  to  $-0.2459$ .

The relative photodebromination rate constants were previously calculated for all 209 PBDEs using our theoretical model [14]. These calculated rate constants were highly correlated with the measured  $\text{Fe}^0$  debromination rate constants for BDE-100, 66, 47, 28, and 7 (Supplemental Data, Fig. S11). This indicates that the rate constants for the two different debromination processes are controlled by the same energy barrier, the C–Br bond dissociation energy.

#### LUMO energies and PBDE debromination rate constants

A linear correlation between the rate constants for  $\text{Fe}^0$  reduction of PBDEs and their LUMO energies was found in a previous study [13]. A good correlation was found between previously published photodebromination rate constants for 15 PBDE congeners [3] and the previously predicted LUMO energies for these same congeners [18] (Supplemental Data, Fig. S-12). These linear relationships indicate that debromination of PBDEs by  $\text{Fe}^0$  treatment and UV light may both be caused by electron transfer. It is easier for the congener with a lower LUMO energy to go to the excited state or accept an electron and, eventually, cleave the C–Br bond.

## CONCLUSION

In comparing the PBDE debromination of photolytic, biological, and chemical processes with our energy-based model, very similar results were found. In almost all cases, the major products are the same for all three processes, with even greater similarity between photodebromination and Fe<sup>0</sup> reduction than with microbial debromination. Results of the present study suggest that chemical debromination kinetics (including photodebromination and Fe<sup>0</sup> debromination) are governed by the enthalpy of formation. It can also be concluded that biotic debromination is generally governed by the same energetic pathways but may be hindered by steric effects of the bromines that do not allow the bacteria to catalyze the most energetically favorable reactions.

Results of the present study show that our energy-based debromination model is a good predictor of the major congeners that can be expected from the photolytic, chemical, and biological debromination of PBDEs. Although the model is able to generally predict the kinetics of actual photolytic and Fe<sup>0</sup> reduction experiments, the model is not able to predict the kinetics of the microbial debromination due to complications of enzymatic and microbial growth considerations. This model can be a useful tool for predicting the major expected debromination products for any PBDE congener released into the environment.

## SUPPLEMENTAL DATA

The supplemental material (Supplemental Figures 1–12) contains details of correlation between experimental results and model predicted results, reaction time profile for debromination products of BDE-197 and octa-BDE mixture, cumulative concentration of the octa-BDE mixture photodebromination and anaerobic biodebromination products, correlation between ln(conc per pathway) and the enthalpy of formation for photodebromination and anaerobic biodebromination. Additionally, the Supplemental Data contains figures of reaction time profile for debromination products of BDE-47 and BDE-209, a figure showing correlation between ln(conc per pathway) and the enthalpy of formation for Fe<sup>0</sup> reduction, and a figure showing correlation between the predicted relative rate constants and experimental Fe<sup>0</sup> debromination rate constants. Finally, there is a figure showing correlation between the calculated LUMO energies and the measured photodebromination rate constants in log format.

*Acknowledgement*—This publication was made possible in part by grant number P30ES00210 from the National Institute of Environmental Health Sciences, National Institute of Health (NIH) through a pilot project awarded by Oregon State University's Environmental Health Sciences Center. Its contents are solely the responsibility of the authors and do not necessarily represent the official view of the NIEHS, NIH. Other funding was provided by the University of California Center for Water Resources grant. The authors would like to acknowledge OSU's EHSC's mass spectrometry core facility for assistance.

## REFERENCES

- Hites RA. 2004. Polybrominated diphenyl ethers in the environment and in people: A meta-analysis of concentrations. *Environ Sci Technol* 38:945–956.
- de Wit CA. 2002. An overview of brominated flame retardants in the environment. *Chemosphere* 46:583–624.
- Eriksson J, Green N, Marsh G, Bergman A. 2004. Photochemical decomposition of 15 polybrominated diphenyl ether congeners in methanol/water. *Environ Sci Technol* 38:3119–3125.
- Bezares-Cruz J, Jafvert CT, Hua I. 2004. Solar photodecomposition of decabromodiphenyl ether: products and quantum yield. *Environ Sci Technol* 38:4149–4156.
- Soderstrom G, Sellstrom U, de Wit CA, Tysklind M. 2004. Photolytic debromination of decabromodiphenyl ether (BDE 209). *Environ Sci Technol* 38:127–132.
- Sanchez-Prado L, Loes M, Llompart M, Garcia-Jares C, Bayona JM, Cela R. 2006. Natural sunlight and sun simulator photolysis studies of tetra- to hexa-brominated diphenyl ethers in water using solid-phase microextraction. *J Chromatogr A* 1124:157–166.
- Rayne S, Ikonou MG, Whale MD. 2003. Anaerobic microbial and photochemical degradation of 4,4'-dibromodiphenyl ether. *Water Res* 37:551–560.
- He J, Robrock KR, Alvarez-Cohen L. 2006. Microbial reductive debromination of polybrominated diphenyl ethers (PBDEs). *Environ Sci Technol* 40:4429–4434.
- Gerecke AC, Giger W, Hartmann PC, Heeb NV, Kohler HP, Schmid P, Zennegg M, Kohler M. 2006. Anaerobic degradation of brominated flame retardants in sewage sludge. *Chemosphere* 64:311–317.
- Gerecke AC, Hartmann PC, Heeb NV, Kohler HP, Giger W, Schmid P, Zennegg M, Kohler M. 2005. Anaerobic degradation of decabromodiphenyl ether. *Environ Sci Technol* 39:1078–1083.
- Darnerud PO, Eriksen GS, Johannesson T, Larsen PB, Viluksela M. 2001. Polybrominated diphenyl ethers: Occurrence, dietary exposure, and toxicology. *Environ Health Perspect Suppl* 109:49–68.
- Johnson TL, Scherer MM, Tratnyek PG. 1996. Kinetics of halogenated organic compound degradation by iron metal. *Environ Sci Technol* 30:2634–2640.
- Keum YS, Li QX. 2005. Reductive debromination of polybrominated diphenyl ethers by zerovalent iron. *Environ Sci Technol* 39:2280–2286.
- Zeng X, Simonich SL, Robrock KR, Korytar P, Alvarez-Cohen L, Barofsky DF. 2008. Development and validation of a congener specific photodegradation model for polybrominated diphenyl ethers. *Environ Toxicol Chem* 27:2427–2435.
- Ackerman LK, Wilson GR, Simonich SL. 2005. Quantitative analysis of 39 polybrominated diphenyl ethers by isotope dilution GC/low-resolution MS. *Anal Chem* 77:1979–1987.
- Korytar P, Covaci A, de Boer J, Gelbin A, Brinkman UA. 2005. Retention-time database of 126 polybrominated diphenyl ether congeners and two bromkal technical mixtures on seven capillary gas chromatographic columns. *J Chromatogr A* 1065:239–249.
- Robrock KR, Korytar P, Alvarez-Cohen L. 2008. Pathways for the anaerobic microbial debromination of polybrominated diphenyl ethers. *Environ Sci Technol* 42:2845–2852.
- Zeng X, Freeman PK, Vasil'ev YV, Voinov VG, Simonich SL, Barofsky DF. 2005. Theoretical calculation of thermodynamic properties of polybrominated diphenyl ethers. *J Chem Eng Data* 50:1548–1556.
- Fennell DE, Nijenhuis I, Wilson SF, Zinder SH, Haeggbloom MM. 2004. Dehalococcoides ethenogenes strain 195 reductively dechlorinates diverse chlorinated aromatic pollutants. *Environ Sci Technol* 38:2075–2081.
- Bedard DL, Ritalahti KM, Loffler FE. 2007. The Dehalococcoides population in sediment-free mixed cultures metabolically dechlorinates the commercial polychlorinated biphenyl mixture Aroclor 1260. *Appl Environ Microbiol* 73:2513–2521.